Single crystalline boron rich B(Al)N alloys grown by MOVPE

P. Vuong, A. Mballo, S. Sundaram, G. Patriarche, Y. Halfaya, S. Karrakchou, A. Srivastava, K. Krishnan, N. Sama, T. Ayari, et al.

Single crystalline boron rich B(Al)N alloys grown by MOVPE

P. Vuong,[1] A. Mballo,[1] S. Sundaram,[1,2] G. Patriarche,[3] Y. Halfaya,[4] S. Karrakchou,[1,2] A. Srivastava,[1,2] K. Krishnan,[1,2] N. Y. Sama,[4] T. Ayari,[1,2] S. Gautier,[4] P. L. Voss,[1,2] J. P. Salvestrini,[1,2] and A. Ougazzaden[1,2,a)]

AFFILIATIONS

[1]Georgia Tech Lorraine, UMI 2958, Georgia Tech–CNRS, 57070 Metz, France

[2]School of Electrical and Computer Engineering, Georgia Institute of Technology, Atlanta, Georgia 30332, USA

[3]Centre de Nanosciences et de Nanotechnologies, Université Paris-Saclay, C2N–Site de Marcoussis, Route de Nozay, F-91460 Marcoussis, France

[4]Institut Lafayette, 2 rue Marconi, 57070 Metz, France

[a)]**E-mail:** abdallah.ougazzaden@georgiatech-metz.fr

Boron rich BAlN alloys have been grown on 2-inch sapphire substrates by Metal-Organic Vapor Phase Epitaxy. The surface morphology of BAlN alloys exhibits a transition stage from a completely two-dimensional to a three-dimensional granular surface with an increased trimethylaluminum/group III (TMAl/III) ratio. Only a shift in the position of the 002 plane reflection peak to higher diffraction angles in the $2\theta - \omega$ scan along with a decrease in intensity was observed, specifying formation of layered BAlN alloys up to a TMAl/III ratio of 14. AlN phase separation was observed while increasing the TMAl/III ratio to 25, supporting SEM observations. Secondary-ion mass spectrometry measurements confirmed the presence of up to 17% Al in layered BAlN alloy systems. A cross sectional transmission electron microscopy (TEM) study confirmed the layered nature of single phase BAlN alloys. It also revealed the presence of wurtzite Al rich BAlN phases in a matrix of layered hexagonal B rich BAlN. Band to band transition around 5.86 eV has been observed, which shifted slightly to lower energy with increasing Al incorporation. The bowing parameter (C) in boron rich BAlN alloy systems was evaluated to be around 0.65 ± 0.05 eV. Encouraging results were obtained on boron rich BAlN alloy formation, motivating further exploration of growth conditions and study of BAlN fundamental properties for applications in deep UV optoelectronics.

Hexagonal boron nitride (h-BN) is a unique III-nitride, which has interesting properties such as a layered structure, high thermal conductivity, and a wide bandgap (~6 eV).[1–5] Even though h-BN is an indirect bandgap semiconductor, it has an impressive deep ultraviolet (UV) emission and, hence, it is very promising for applications in deep UV optoelectronics when compared to direct bandgap AlN and other materials.[3,6–13] The AlN alloy system, on the other hand, is the most studied material for applications in the deep UV regime, but growth of high quality materials and p-type doping are challenging.[6,14] Both Al rich w-BAlN and B rich h-BAlN alloys may enable a desirable bandgap and lattice/strain engineering for applications. For example, h-BN can be made into a direct bandgap material through strain engineering or alloying with Al, which would enhance emission efficiency in the deep UV for UV LEDs. Alloying boron into AlN could also lead to a type II BAlN/AlGaN heterojunction,[15] allowing the achievement of an electron blocking layer. BAlN has also been studied as a promising material candidate for high-reflectivity distributed Bragg reflectors (DBRs) due to strong refractive index modification.[16,17] Because of their layered nature and reported intrinsic p-type behavior, the use of h-BN based alloys may give more flexibility to design highly efficient device structures.[18–20] Theoretically, it was reported that BAlN alloys can have structural crossover from hexagonal to wurtzite at 50% of boron, and the band-gap transition from indirect to direct would occur at 75% of boron.[21,22]

Apart from these theoretical investigations, boron rich BAlN alloys have not yet been explored experimentally. The growth of boron rich BAlN alloys and the understanding of its basic structural, as well as the optical, properties are of high importance. In this work, we report growth of single-phase boron rich BAlN alloys up to 17% of Al in a Metal-Organic Vapor Phase Epitaxy (MOVPE) reactor. We first studied in detail the relationship between morphology, Al composition, and the trimethylaluminum/group III (TMAl/III) ratio. Second, the bandgap variation in boron rich BAlN and the bowing effect were presented.

The BAlN alloys were grown directly on c-plane sapphire substrates without any buffer in an Aixtron MOVPE close coupled showerhead (CCS) reactor. Triethylboron (TEB), trimethylaluminum (TMAl), and ammonia (NH_3) were precursors for boron, aluminum, and nitrogen, respectively. 20 nm thick of BAlN layers were grown at 1280 °C and 90 mbar pressure. The TMAl/III ratio was varied from 0 to 25; in order to increase the Al content in gas phase, all other parameters were kept constant.

A scanning electron microscope (SEM) was used to study the surface morphology of the samples. The crystalline structure and phase purity of BAlN alloys were examined by high-resolution X-ray diffraction (HRXRD) scans, performed in a Panalytical X'pert Pro Materials Research Diffractometers system with Cu Kα radiation in triple axis mode. The aluminum content was estimated by Secondary-ion mass spectrometry (SIMS) using Cs+ molecular ions. The interfaces of heterostructures were characterized by high-angle Annular Dark Field Scanning Transmission electron Microscopy (HAADF-STEM) performed on an aberration-corrected JEOL 2200FS electron transmission microscope. Prior to this study, cross sectional lamellae were prepared by the FIB process after coating a 100 nm thick carbon for layer protection. Transmission spectra were measured at room temperature with a Perkin Elmer LAMBDA 950 spectrophotometer.

The surface morphology of BAlN alloys grown on sapphire substrates with four different TMAl/III ratios is shown in Fig. 1. At a low TMAl/III ratio [Figs. 1(a) and 1(b)], we observe honeycomb like wrinkles on the surface, which is comparable with the standard morphology of un-alloyed 2D h-BN. The formation of the wrinkles is the consequence of the compressive stress from cooling process as reported earlier by Li *et al.*[1] This morphology confirms that these samples are completely layered. When the TMAl/III ratio is increased, these wrinkles are less pronounced and small grains were obtained as seen in Fig. 1(c). Subsequently at a higher TMAl/III ratio of 25, the morphology of the BAlN alloy consists of 3D grains with complete absence of wrinkles [Fig. 1(d)]. The 2D–3D transition of the morphology reveals the influence of the TMAl/III ratio on the surface of BAlN alloys. Further characterization has been performed to understand the structural changes of these BAlN alloys.

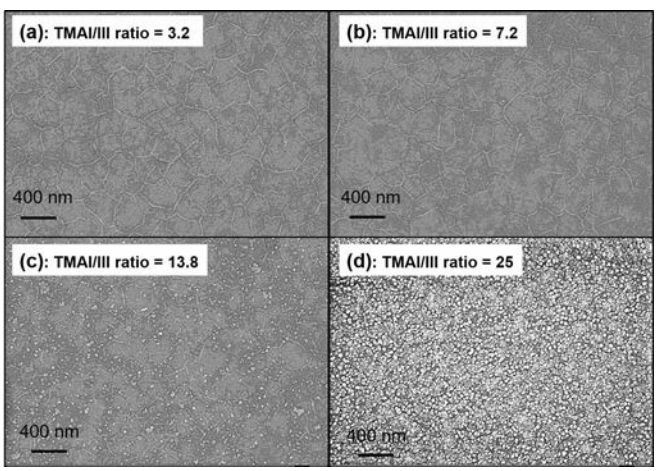

FIG. 1. SEM images of BAlN alloys grown on sapphire with four different TMAl/III ratios. (a) 3.2, (b) 7.2, (c) 13.8, and (d) 25.

Figure 2(a) shows High-Resolution X-Ray diffraction (HR-XRD) of the 20 nm thick BAlN alloys grown with the different TMAl/III ratio. We have observed only the diffraction peak at around 26.0° for samples with the TMAl/III ratio from 0 to 13.8, which confirms the formation of layered BAlN alloys. At a TMAl/III ratio of 25, in addition to the h-BN peak, the $2\theta-\omega$ scan showed the presence of a second peak at 35.9° corresponding to the (002) w-AlN. The observation of the two peaks indicates the phase separation in this sample. By increasing the TMAl/III ratio, the position of the (002) h-BN peak is found to be shifted toward a higher angle (by 0.2 °), except the BAlN alloy grown with the highest of TMAl/III ratio due to the phase separation [inset of Figs. 2(a) and 2(b)]. Because the boron (B) atoms are smaller than aluminum (Al), adding the Al into the h-BN layer can give rise to the local tensile stress. This stress will lead to the increase in the lattice parameter *a* and the decrease in the lattice parameter *c*. According to Bragg's law, the crystal lattice *c*, in our study, is calculated to decrease from 6.92 Å (for pure h-BN) to 6.86 Å (for BAlN alloy grown with a TMAl/III ratio of 13.8). This decrement indicates the increase in the Al content in our BAlN alloys. In the case of the phased separated sample, the h-BN (AlN) peak was found to be shifted (around 0.05 °) to the higher (lower) angle, compared to the reported values.[1,23] We attribute this shift to the presence of the BAlN alloy. High resolution TEM and SIMS measurements will be discussed later for a more complete study of this sample. In addition to this shift, the full width half-maximum (FWHM) of the h-BN diffraction peak increases linearly with the TMAl/III ratio [Fig. 2(c)]. This broadened FWHM is related to the incorporation of Al into the h-BN layer. These results are evidence confirming the formation of BAlN alloys and the Al content increases with the TMAl/III ratio.

To estimate the efficiency of Al incorporation into our BAlN alloys, secondary-ion mass spectrometry (SIMS) measurements were performed. Figure 3(a) shows SIMS elemental concentration depth profiles of aluminum atoms in BAlN alloys with five different TMAl/III ratios. In the first 5 nm depth, there is a thin silver layer which was deposited on the top of the 20 nm thick BAlN for charge compensation purpose during the SIMS analysis, and the interface between the coated layer and BAlN alloys. The region from 20 nm to 40 nm depth is a transition zone between BAlN alloys and sapphire substrates, which give a higher value of Al concentration. Our measurements and analysis were focused in the region between 5 nm and ∼20 nm depth (flat part). We found that the Al concentration is increasing with the enhancement of the TMAl/III ratio from 0 to 25. At the TMAl/III ratio of 25, the Al concentration reaches the same level with the one derived from sapphire substrate (25–40 nm depth) due to the phase separation as demonstrated by HR-XRD. In this sample therefore, we may find some areas with Al rich BAlN or even pure w-AlN. Figure 3(b) plots the estimation of Al composition from 0% (pure h-BN) to 100% (pure w-AlN) as a function of the TMAl/III ratio. We obtained the Al content of 1%, 3.5%, and 17% for the TMAl/III ratios of 3.2, 7.2, and 13.8, respectively. In the case of the TMAl/III ratio of 25, the specific value of Al content could not be evaluated accurately due to the non-homogeneity of the layer (phase separation). Details of Al and B contents in this alloy have been further investigated in the following STEM and EDX analysis section. To interpret this, our experimental data were fitted by using the Lorentz function [green solid line in Fig. 3(b)]. At a low TMAl/III ratio ($\leq$14), the fit gives a good agreement with our data, confirming the enhancement of Al incorporation

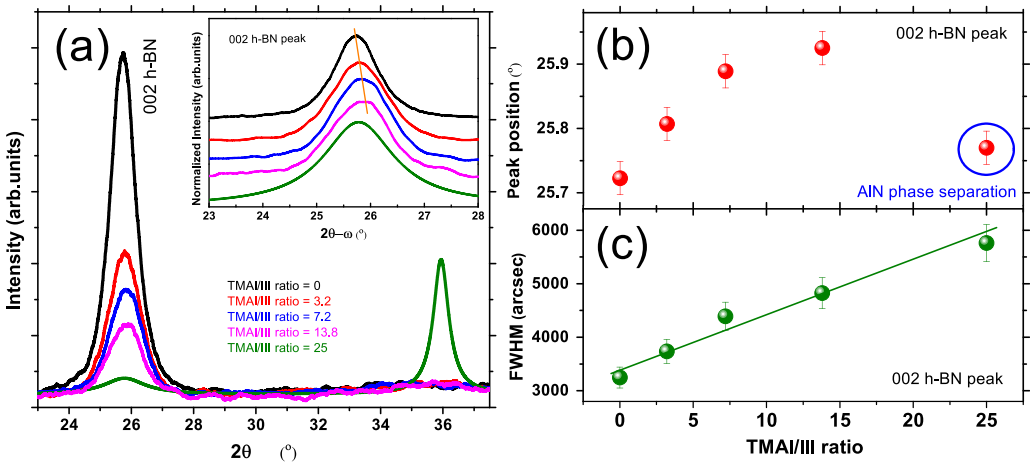

FIG. 2. (a) High-Resolution X-Ray Diffraction (HR-XRD) $2\theta - \omega$ scan of the BAlN alloys grown on sapphire with five different TMAl/III ratios. The inset shows a clear shift of the 002 h-BN peak toward a higher angle. (b) and (c): The 002 h-BN peak position and full width half-maximum (FWHM) as a function of TMAl/III ratio, respectively.

when the TMAl/III ratio is increased. However, when the TMAl/III ratio is higher than 25, the Al composition starts being saturated. We attribute that this saturation is due to the phase separation between BN and AlN as also investigated by HR-XRD. Therefore, in this study the maximum composition of Al in BAlN on sapphire without phase separation is up to 17%. Compared to the theoretical value of BAlN on AlN, this experimental value is higher than 9% predicted in Ref. 24 and lower than in Ref. 21.

As direct evidence of the crystal phase, the cross section high-resolution TEM images of 20 nm BAlN alloys grown with the TMAl/III ratio of 3.2 and 25 are shown in Figs. 4(a) and 4(b). At a low Al content, the TEM image exhibits a uniform crystalline growth feature with the lattice oriented along the c-axis [Figs. 4(a)]. The BAlN alloy forms a 2D layered structure from the beginning without generating any dislocations, which indicates a good quality of this alloy. The inset of Fig. 4(a) presents the fast Fourier transform (FFT) pattern, corresponding to the selected area indicated by a white box. It can be clearly identified as a single crystalline hexagonal phase of the BAlN alloy, in agreement with the HR-XRD measurement. The TEM image and FFT pattern in the inset for the different areas of the sample grown with a TMAl/III ratio of 25 are shown in Fig. 4(b). In the beginning of the growth, the hexagonal BAlN alloy was formed as identified from the FFT pattern. Then, the wurtzite BAlN forms. The wurtzite BAlN layers are confined in short domains and irregularly oriented, losing the long range order. This confirms the phase separation occurring in this sample as already investigated by HR-XRD and SIMS. To deeply understand this feature, we recorded the complementary cross section high-angle annular dark field scanning transmission electron microscopy (HAADF-STEM) image and the energy dispersive X-ray spectroscopy (EDX) element mappings of Al and B for this sample as presented in Fig. 4(c). Five different zones were selected [green boxes in Fig. 4(c)] to estimate the element contents of B and Al atoms in this BAlN alloy. The results of B and Al atoms for each corresponding zone are shown in Table I. Zone 1 has 64% Al and the content of B is below

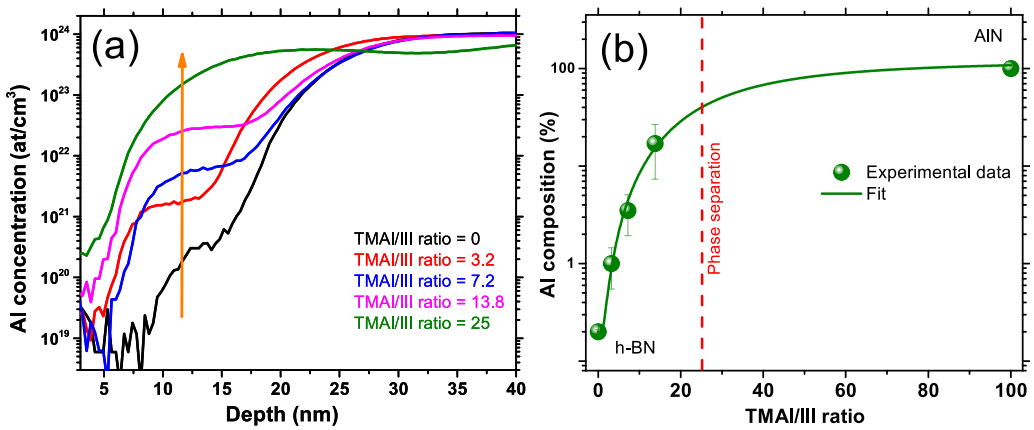

FIG. 3. (a) SIMS elemental concentration depth profiles of Al for the BAlN alloys grown on sapphire with four different TMAl/III ratios; (b) Al composition as a function of TMAl/III ratio.

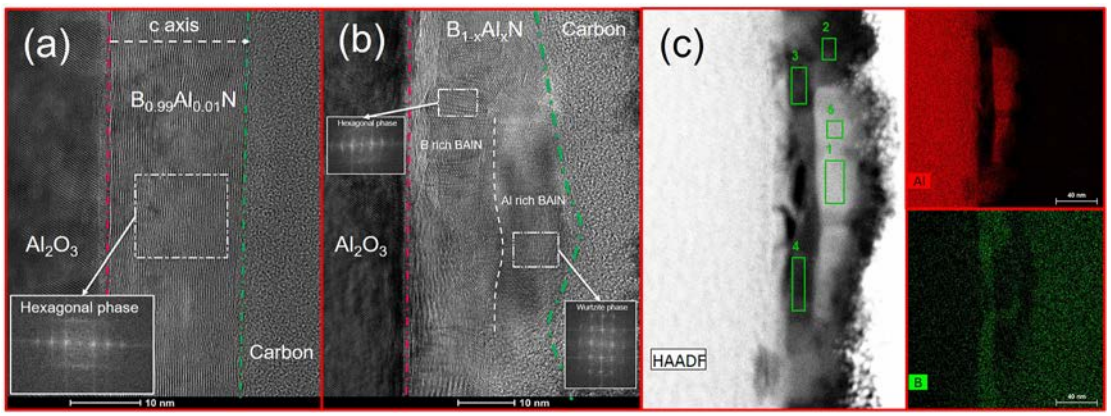

FIG. 4. Cross section high-resolution TEM image of 20 nm BAlN grown on sapphire with the TMAl/III ratios of (a) 3.2 and (b) 25; (c) bright-field HAADF-STEM image of BAlN grown on sapphire with a TMAl/III ratio of 25 and the energy dispersive X-ray spectroscopy (EDX) elemental mappings of Al and B.

TABLE I. Content of Al and B elements in the different zone of the BAlN alloy grown on sapphire with a TMAl/III ratio of 25.

	Wt.%				
Element	Zone 1	Zone 2	Zone 3	Zone 4	Zone 5
Al	∼64	∼5	∼7	∼7	∼49
B	Below the detection limit	∼44	∼44	∼42	∼17

the detection limit, indicating a pure w-AlN crystallite formed which is in agreement with SIMS measurement. From zone 2 to zone 4, B rich BAlN alloys were obtained with around 44% of B and 5%–7% of Al, supporting the hexagonal phase. However, in zone 5, 49% of Al and 17% of B were found, indicating the Al rich BAlN alloy in this area. We thus conclude that in this sample, there is a matrix of the Al rich BAlN in the wurzite phase and the B rich BAlN in the hexagonal phase together with the pure w-AlN.

Transmission spectroscopy was utilized to investigate the bandgap variation in the BAlN layers. Figure 5(a) shows transmission spectra, which were recorded at room temperature for the three different Al compositions of the BAlN alloys. All spectra exhibit a light shift to higher wavelengths with an increase in Al content. The squared absorption coefficient (α^2), which was calculated from these transmission measurements, is plotted as a function of the photon energy as seen in the inset of Fig. 5(a). A well-defined linear behavior is observed in the high-energy side (dashed line in the inset of Fig. 5). The optical bandgap of those samples was estimated based on the basic equation: $\alpha^2 = \alpha_0^2 (E - E_g)$. We obtain a shift to lower energy from 5.86 eV to 5.82 eV when the Al content is increased from 1% up to 17%. The redshift of the bandgap in our alloys can be understood using the bandgap bowing concept. Figure 5(b) plots our estimated bandgap of BAlN alloys vs the Al composition (blue sphere) together with the fit (red line) using a modified Vegard's law: $E_g = (1-x)E_g^{h-BN} + xE_g^{w-AlN} - Cx(1-x)$

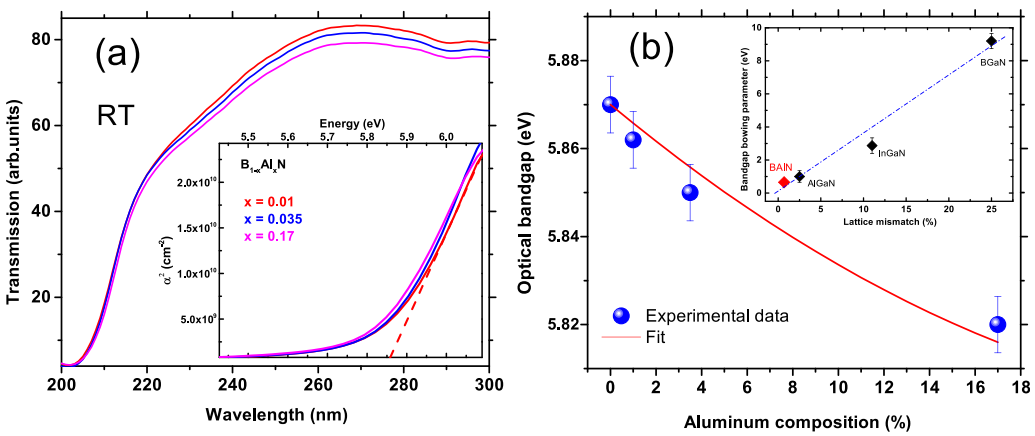

FIG. 5. (a) Transmission spectra of the $B_{1-x}Al_xN$ grown on the sapphire substrate with different Al compositions. Inset: the squared absorption coefficient (α^2) vs photon energy for estimating energy bandgap; (b) bandgap variation vs Al composition. Inset: bandgap bowing parameters for nitride compounds vs the lattice mismatch between the end point binaries. Data for AlGaN is from Ref. 26, for InGaN is from Ref. 27, and for BGaN is from Ref. 28.

where C is the bowing parameter. In our fit, the bandgap of AlN = 6.12 eV,[14] the optical gap of h-BN = 5.87 eV,[1] and we obtained the bowing parameter C = 0.65 ± 0.05 eV. The relatively low value of C in BAlN may be attributed to the small difference between the indirect gap of h-BN and the direct gap of AlN. Thus, the alloy bandgap exhibits only small deviation from linear interpolation. It is in agreement with the theoretical study of BGaN alloys. Turiansky *et al.* reported a bowing parameter of 0.55 eV for the indirect bandgap of BGaN.[25] In addition, the comparison of our value C = 0.65 ± 0.05 eV with the recommended bowing parameters for other nitride-based systems is considered. The inset of Fig. 5(b) illustrates the general trend for the bandgap bowing parameter in the III-nitride alloy systems by presenting C value vs the lattice mismatch between the end point binaries: AlGaN (C = 1 eV[26]) InGaN (C = 2.87 eV[27]) BGaN (C = 9.2 eV[28]), and BAlN. Our experimental value of C = 0.65 ± 0.05 eV thus is in a reasonable range of the bowing parameters for nitride compounds.

In summary, boron rich BAlN alloys have been grown by Metal-Organic Vapor Phase Epitaxy (MOVPE). The surface of BAlN alloys presents a morphology ranging from a completely 2-dimensional (2D) to a three-dimensional (3D) granular surface with increasing Al content. The HR-XRD study shows only a shift in the position of the 002 plane reflection peak to higher diffraction angles, which indicates single hexagonal phase BAlN alloys up to a TMAl/III ratio of 14. Further increases of the TMAl/III ratio up to 25 resulted in phase separation. The Al composition in the BAlN layer was estimated by SIMS to be up to 17%. The TEM study confirmed the layered nature in single phase BAlN alloys. It also revealed the presence of wurtzite Al rich BAlN phases in a matrix of layered hexagonal B rich BAlN. Band to band transition around 5.86 eV has been observed, which shifted slightly to lower energy with increasing Al incorporation. The bowing parameter (C) in the boron rich BAlN alloy system was evaluated to be around 0.65 ± 0.05 eV. The growth of flexible boron rich B(Al)N alloys brings a new alloy for the next generation of the nitride family, which is very promising for the development of applications such as deep UV LEDs.

This study was partially funded by the French PIA project Lorraine Université d'Excellence (Grant No. ANR-15-IDEX-04-LUE) and French National Research Agency (ANR) under the GANEX Laboratory of Excellence (Labex) project (Grant No. ANR-11-LABX-0014). The authors gratefully acknowledge Dr. J. Zaraket and Dr. C. Chevallier from CentraleSupelec/LMOPS for their help on transmission measurements. We would like to thank Professor X. Li, Dr. T. Tran from King Abdullah University of Science and Technology (KAUST), and Professor B. Gil, C. Elias from Laboratoire Charles Coulomb (L2C), University of Montpellier for fruitful discussions about characterization.

REFERENCES

[1]X. Li, S. Sundaram, Y. E. Gmili, T. Ayari, R. Puybaret, G. Patriarche, P. L. Voss, J. P. Salvestrini, and A. Ougazzaden, Cryst. Growth Des. **16**, 3409 (2016).
[2]K. Watanabe, T. Taniguchi, and H. Kanda, Nat. Mater. **3**, 404 (2004).
[3]G. Cassabois, P. Valvin, and B. Gil, Nat. Photonics **10**, 262 (2016).
[4]H. X. Jiang and J. Y. Lin, ECS J. Solid State Sci. Technol. **6**, Q3012 (2017).
[5]T. Taniguchi and K. Watanabe, J. Cryst. Growth **303**, 525 (2007).
[6]H. X. Jiang and J. Y. Lin, Semicond. Sci. Technol. **29**, 084003 (2014).
[7]T. Q. P. Vuong, G. Cassabois, P. Valvin, V. Jacques, A. V. D. Lee, A. Zobelli, K. Watanabe, T. Taniguchi, and B. Gil, 2D Mater. **4**, 011004 (2016).
[8]K. Watanabe, T. Taniguchi, T. Niiyama, K. Miya, and M. Taniguchi, Nat. Photonics **3**, 591 (2009).
[9]Y. Kubota, K. Watanabe, O. Tsuda, and T. Taniguchi, Science **317**, 932 (2007).
[10]L. Schué, L. Sponza, A. Plaud, H. Bensalah, K. Watanabe, T. Taniguchi, F. Ducastelle, A. Loiseau, and J. Barjon, Phys. Rev. Lett. **122**, 067401 (2019).
[11]H. Liu, J. Meng, X. Zhang, Y. Chen, Z. Yin, D. Wang, Y. Wang, J. You, M. Gao, and P. Jin, Nanoscale **10**, 5559 (2018).
[12]C.-H. Lin, H.-C. Fu, B. Cheng, M.-L. Tsai, W. Luo, L. Zhou, S.-H. Jang, L. Hu, and J.-H. He, Npj 2D Mater. Appl. **2**(1), 23 (2018).
[13]M. Gao, J. Meng, Y. Chen, S. Ye, Y. Wang, C. Ding, Y. Li, Z. Yin, X. Zeng, J. You, P. Jin, and X. Zhang, J. Mater. Chem. C **7**, 14999 (2019).
[14]J. Li, K. B. Nam, M. L. Nakarmi, J. Y. Lin, H. X. Jiang, P. Carrier, and S.-H. Wei, Appl. Phys. Lett. **83**, 5163 (2003).
[15]H. Sun, Y. J. Park, K.-H. Li, C. Castanedo, A. Alowayed, T. Detchprohm, R. Dupuis, and X. Li, Appl. Phys. Lett. **111**, 122106 (2017).
[16]M. Abid, T. Moudakir, G. Orsal, S. Gautier, A. En Naciri, Z. Djebbour, J.-H. Ryou, G. Patriarche, L. Largeau, H. J. Kim, Z. Lochner, K. Pantzas, D. Alamarguy, F. Jomard, R. D. Dupuis, J.-P. Salvestrini, P. L. Voss, and A. Ougazzaden, Appl. Phys. Lett. **100**, 051101 (2012).
[17]X. Li, S. Wang, H. Liu, F. A. Ponce, T. Detchprohm, and R. D. Dupuis, Phys. Status Solidi B **254**, 1600699 (2017).
[18]T. Ayari, S. Sundaram, X. Li, Y. E. Gmili, P. L. Voss, J. P. Salvestrini, and A. Ougazzaden, Appl. Phys. Lett. **108**, 171106 (2016).
[19]Y. Kobayashi, K. Kumakura, T. Akasaka, and T. Makimoto, Nature **484**, 223 (2012).
[20]H. Srour, J. P. Salvestrini, A. Ahaitouf, S. Gautier, T. Moudakir, B. Assouar, M. Abarkan, S. Hamady, and A. Ougazzaden, Appl. Phys. Lett. **99**, 221101 (2011).
[21]T. Akiyama, K. Nakamura, and T. Ito, Appl. Phys. Express **11**, 025501 (2018).
[22]J.-X. Shen, D. Wickramaratne, and C. Van de Walle, Phys. Rev. Mater. **1**, 065001 (2017).
[23]X. Li, S. Sundaram, Y. E. Gmili, T. Moudakir, F. Genty, S. Bouchoule, G. Patriarche, R. D. Dupuis, P. L. Voss, J.-P. Salvestrini, and A. Ougazzaden, Phys. Status Solidi A **212**, 745 (2015).
[24]Y. Hasegawa, T. Akiyama, A.-M. Pradipto, K. Nakamura, and T. Ito, Jpn. J. Appl. Phys., Part 1 **58**, SCCB21 (2019).
[25]M. E. Turiansky, J.-X. Shen, D. Wickramaratne, and C. G. Van de Walle, J. Appl. Phys. **126**, 095706 (2019).
[26]I. Vurgaftman, J. R. Meyer, and L. R. Ram-Mohan, J. Appl. Phys. **89**, 5815 (2001).
[27]G. Orsal, Y. E. Gmili, N. Fressengeas, J. Streque, R. Djerboub, T. Moudakir, S. Sundaram, A. Ougazzaden, and J. P. Salvestrini, Opt. Mater. Express **4**, 1030 (2014).
[28]A. Ougazzaden, S. Gautier, T. Moudakir, Z. Djebbour, Z. Lochner, S. Choi, H. J. Kim, J.-H. Ryou, R. D. Dupuis, and A. A. Sirenko, Appl. Phys. Lett. **93**, 083118 (2008).